Science Translational Medicine
AAAS

stm.sciencemag.org/cgi/content/full/13/581/eabf0891/DC1

Supplementary Materials for

Exercise triggers CAPN1-mediated AIF truncation, inducing myocyte cell death in arrhythmogenic cardiomyopathy

Stephen P. Chelko*, Gizem Keceli, Andrea Carpi, Nunzianna Doti, Jacopo Agrimi, Angeliki Asimaki, Carlos Bueno Beti, Matthew Miyamoto, Nuria Amat-Codina, Djahida Bedja, An-Chi Wei, Brittney Murray, Crystal Tichnell, Chulan Kwon, Hugh Calkins, Cynthia A. James, Brian O'Rourke, Marc K. Halushka, Edon Melloni, Jeffrey E. Saffitz, Daniel P. Judge, Menotti Ruvo, Richard N. Kitsis, Peter Andersen, Fabio Di Lisa, Nazareno Paolocci*

*Corresponding author. Email: stephen.chelko@med.fsu.edu (S.P.C.), npaoloc1@jhmi.edu (N.P.)

Published 17 February 2021, *Sci. Transl. Med.* **13**, eabf0891 (2021)
DOI: 10.1126/scitranslmed.abf0891

The PDF file includes:

Other Supplementary Material for this manuscript includes the following:

(available at stm.sciencemag.org/cgi/content/full/13/581/eabf0891/DC1)

Data file S1 (Microsoft Excel format). Raw data.

Supplemental Materials and Methods

Electron paramagnetic resonance

Stock solutions of 1-hydroxy-3-methoxycarbonyl-2,2,5,5-tetramethylpyrrolidine hydrochloride (CMH; Enzo Life Sciences, Farmingdale, NY) were prepared daily in nitrogen-purged 0.9% (w/v) NaCl, 25 g/L Chelex 100 (Bio-Rad), and 0.1 mM diethylenetriaminepentaacetic acid (DTPA), and kept on ice. Left and right ventricular tissues were homogenized in phosphate-buffered saline (PBS) containing 0.1 mM DTPA and protease inhibitor cocktail (Roche Applied Science, Indianapolis, IN) at pH 7.4. Insoluble fractions were removed by centrifugation at 15,000 *g* for 10 min (4^{o}C). Homogenates were kept on ice and analyzed immediately. Samples were treated with 1 mM CMH at 37^{o}C for 2 min, transferred to 0.05 ml glass capillary tubes, and analyzed on a Bruker E-Scan (Billerica, MA) electron paramagnetic resonance (EPR) spectrometer. EPR spectrometer settings were as follows: sweep width, 100 G; microwave frequency, 9.75 GHz; modulation amplitude, 1 G; conversion time, 5.12 ms; receiver gain, 2 x 10^{3}; the number of scans, 16. EPR signal intensities were normalized with respect to tissue homogenate protein concentrations as determined by the Pierce BCA protein assay kit (Life Technologies).

Immunoblotting

Ventricular myocardia, HL-1 cells, and mouse ESC-CMs were lysed in RIPA buffer containing 1:100 phosphatase and proteinase inhibitor cocktails (Sigma-Aldrich), and centrifuged according to the protocols described below to isolate soluble, insoluble, and mitochondrial or nuclear proteins. Protein lysates were quantified by standard Pierce BCA protein assay kit (Life Technologies). Forty micrograms of protein lysates were separated on either 4 – 12% or 12% BisTris gels (NuPage, Invitrogen) under non-denaturing conditions with 1X MOPS Running Buffer (Invitrogen). Following transfer to nitrocellulose membranes and blocking (1 hour in 1× PBS containing 5% nonfat milk and 0.1% Tween-20) at room temperature, immunoblots were probed with primary antibodies overnight at 4°C in blocking buffer. Primary antibodies, corresponding product numbers and concentrations used were as follows: Rabbit monoclonal against AIF (Cell Signaling, 5318S, at 1:3,000); rabbit monoclonal against GAPDH (Cell Signaling, 5174, at 1:10,000); rabbit monoclonal against TXN2 (Cell Signaling, 14907S, at 1:1,000); mouse monoclonal against TXNRD2 (Cell Signaling, 12029S, at 1:1,000); rabbit monoclonal against TXN1 (Cell Signaling, 2429S, at 1:1,000); rabbit monoclonal against TXNRD1 (Cell Signaling, 15140S, at 1:1,000); rabbit monoclonal against cytC (Cell Signaling, 4280S, at 1:3,000); rabbit

polyclonal against PRDX3 (Thermofisher, LF-PA0030, at 1:3,000); rabbit polyclonal against CAPN1 (Cell Signaling, 2556S, at 1:1000); mouse monoclonal against CAPN1 Domain III (ThermoFisher, MA3-940, at 1:1000); rabbit polyclonal against CAPN2 (Cell Signaling, 2539S, at 1:1,000), rabbit monoclonal against Histone-3 (Cell Signaling, 4499S, at 1:3,000), rabbit polyclonal against β-actin (Abcam, ab8227, at 1:5,000), rabbit polyclonal against PARP-1 (BioMol, P3113-20F, at 1:1,000), rabbit polyclonal against caspase-3 (Cell Signaling, 9662, at 1:1,000), mouse monoclonal against OPA1 (BD Transduction Laboratories, 612606, at 1:1,000), mouse monoclonal against Calnexin (BD Transduction Laboratories, 610524, at 1:10,000), mouse monoclonal against plasma membrane Na^+/K^+-ATPase (Abcam, ab76020, at 1:1,000), rat monoclonal against Lamp2 (Millipore, 428019, at 1:500); mouse monoclonal against MAO-A (Santa Cruz, sc-271123, at 1:1,000); and rabbit polyclonal against COXIV (ThermoFisher, 11242-1-AP, at 1:5,000). The following day, immunoblots were washed three times (1× PBS) and probed with species-specific IRDye secondary antibodies (Li-Cor IRDye 800CW or IRDye 680RD at 1:10,000; or HRP-conjugate at 1:10,000) for 1 hour at room temperature in blocking buffer. Immunoblots were then washed three times, and immunoblot images were obtained with the LI-COR Odyssey imaging system.

Immunohistochemical and immunofluorescence staining

All myocardia (sedentary and exercised mouse cohorts, and patient myocardial biopsies) were formalin-fixed and paraffin-embedded (FFPE). Slides were obtained from FFPE blocks (5 μm thick), then were deparaffinized, were rehydrated, underwent antigen retrieval, and were blocked for 1 hour at room temperature, then were incubated with primary antibodies at 4^{o}C overnight as previously described (*8*). The following primary antibodies were used: rabbit monoclonal against AIF (Cell Signaling, 5318S, at 1:250), mouse monoclonal against cardiac Troponin-T (cTnT; Thermofisher, MA5-12960, at 1:500), and rabbit polyclonal against HMGB1 (Thermofisher, PA1-16926, at 1:100). Slides were then washed three times with 1× PBS and probed with species-specific Alexa Fluor secondaries or for 1 hour at room temperature (ThermoFisher, donkey anti-mouse Alexa Fluor 488, R37114, at 1:1,000; and donkey anti-rabbit Alexa Fluor 594, R37119, at 1:1,000). Following three additional washes, ProLong Gold Antifade Mountant with DAPI (Thermofisher, 936931) were applied, and coverslips were applied, and immunoreactive signal was detected by laser scanning microscopy (Zeiss LSM 510 Meta). Additionally, Masson's trichrome, H&E, and COX IV (ThermoFisher, 11242-1-AP, at 1:500) immunohistochemistry sections were imaged on an Olympus BX51TF with a DP70 color camera (Olympus).

Thioredoxin reductase activity

Stock solutions of NADPH (48 mM) and 5,5'-dithio-bis-[2-nitrobenzoic acid] (DTNB, 100 mM) were prepared in MilliQ water and DMSO, respectively. Flash-frozen ventricular tissue was homogenized in 0.1 M potassium phosphate buffer containing 0.1 mM DTPA and protease inhibitor cocktail at pH 7.0. The samples were then subjected to three sequential freeze/thaw cycles between liquid nitrogen and 37^{o}C water bath. The insoluble fractions were removed by centrifugation at 14,000 x g for 2 min at 4^{o}C, and the protein concentrations were quantified by BCA assay (Pierce). Briefly, the homogenates (0.1 mg/ml) were incubated with 0.24 mM NADPH and 3 mM DTNB in pH 7.0 potassium phosphate buffer in the presence or absence of thioredoxin reductase inhibitor, auranofin (100 nM), for 2 hrs at room temperature in the dark. The relative absorbance of 2-nitro-5-thiobenzoate anion (TNB^{2-}, ε_{412} = 14150 $M^{-1}cm^{-1}$) was detected on a SpectraMax microplate reader (Molecular Devices) at baseline and following 2 hr incubation. In all cases, each sample was analyzed in triplicate, and total TXNRD activity was calculated. One unit of TXNRD activity is the amount of enzyme that generates 1.0 µmol of TNB^{2-} per minute at 25°C.

Mass tag labeling

Two hundred micrograms of mouse ventricular protein were incubated with either (i) control solution (RIPA alone) or (ii) 1 mM methoxypolyethylene glycol maleimide (mPEG) in RIPA for 2hrs at room temperature, in the dark, with rotation. Protein pellets were precipitated by sequential addition of methanol (400 µl), chloroform (150 µl), deionized water (300 µl) and then centrifuged (20,000 x *g* for 5 mins at 4^{o}C, in the dark). The supernatant was discarded and protein pellets were washed with 400 µl methanol and centrifuged at 20,000 x *g* for 5 mins at 4^{o}C in the dark, and the supernatant was discarded. Protein pellets were resuspended in 50 µl of loading buffer containing 1X dithiothreitol (Invitrogen), heated to 95^{o}C for 10 mins, and 40 µg of control and mPEG-treated samples were run on 4 – 12% or 12% BT gels under non-reducing conditions. All mPEG-labeled protein bands from a single lysate were normalized against their corresponding non-mPEGged labeled bands from that exact same lysate (non-mPEG incubated lysates). As an example, lanes 1 and 4 in Figure 7B utilize the exact same protein lysate, from the exact same mouse, with the exact same protein concentration. Yet, lane 4 was pre-treated with 1 mM mPEG. Thus, protein bands observed in lane 4 (i.e., “mAIF (77kDa); mPEGged ■" and "mAIF (62kDa) ■") are normalized to lane 1 "mAIF (62kDa) ■" bands. Each protein band in the oxidized state (non-mPEGged) and reduced-state (i.e., mPEGged) were divided by the corresponding untreated bands, then all bands (oxidized and reduced) were calculated as a percentage of the sum.

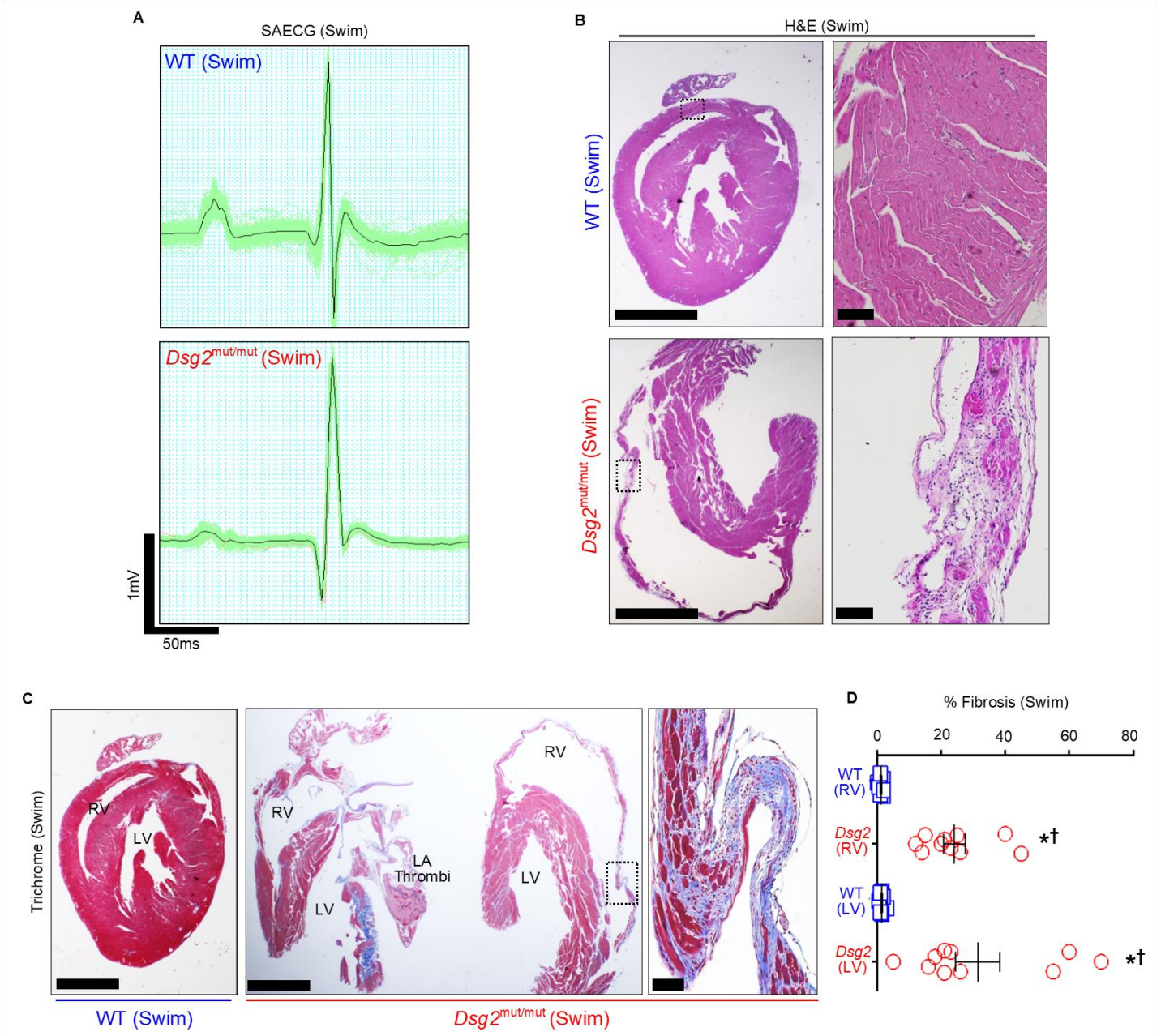

Fig. S1. *Dsg2*$^{mut/mut}$ mice display ECG abnormalities and myocardial injury in response to endurance exercise. (**A**) Representative 90 min signal averaged ECGs (SAECGs) from exercised mice at swim endpoint. Data are representative of n ≥ 13 mice/genotype (see table S1 for quantified data). (**B**) Hematoxylin & Eosin (H&E) staining to visualize morphology and immune cell infiltration of myocardium from exercised *Dsg2*$^{mut/mut}$ and WT mice. (**C**) Masson's Trichrome staining to visualize fibrotic tissue in myocardium from exercised mice. Data are representative of n ≥ 14 mice/genotype. In B and C, large scale bars = 1 mm, small scale bar = 100 µm; enlarged images are from regions in dotted black boxes in adjacent images. (**D**) Quantification of fibrotic areas in right ventricle (RV) and left ventricle (LV) in *Dsg2*$^{mut/mut}$ mouse and WT mouse hearts. Data are presented as mean ± SEM (n ≥ 10 mice/genotype/parameter). *, P < 0.05 *Dsg2*$^{mut/mut}$ (%LV and %RV fibrosis) compared to WT %LV fibrosis; †, P < 0.05 *Dsg2*$^{mut/mut}$ (%LV and %RV fibrosis) compared to WT %RV fibrosis, using One-way ANOVA with Tukey post-hoc.

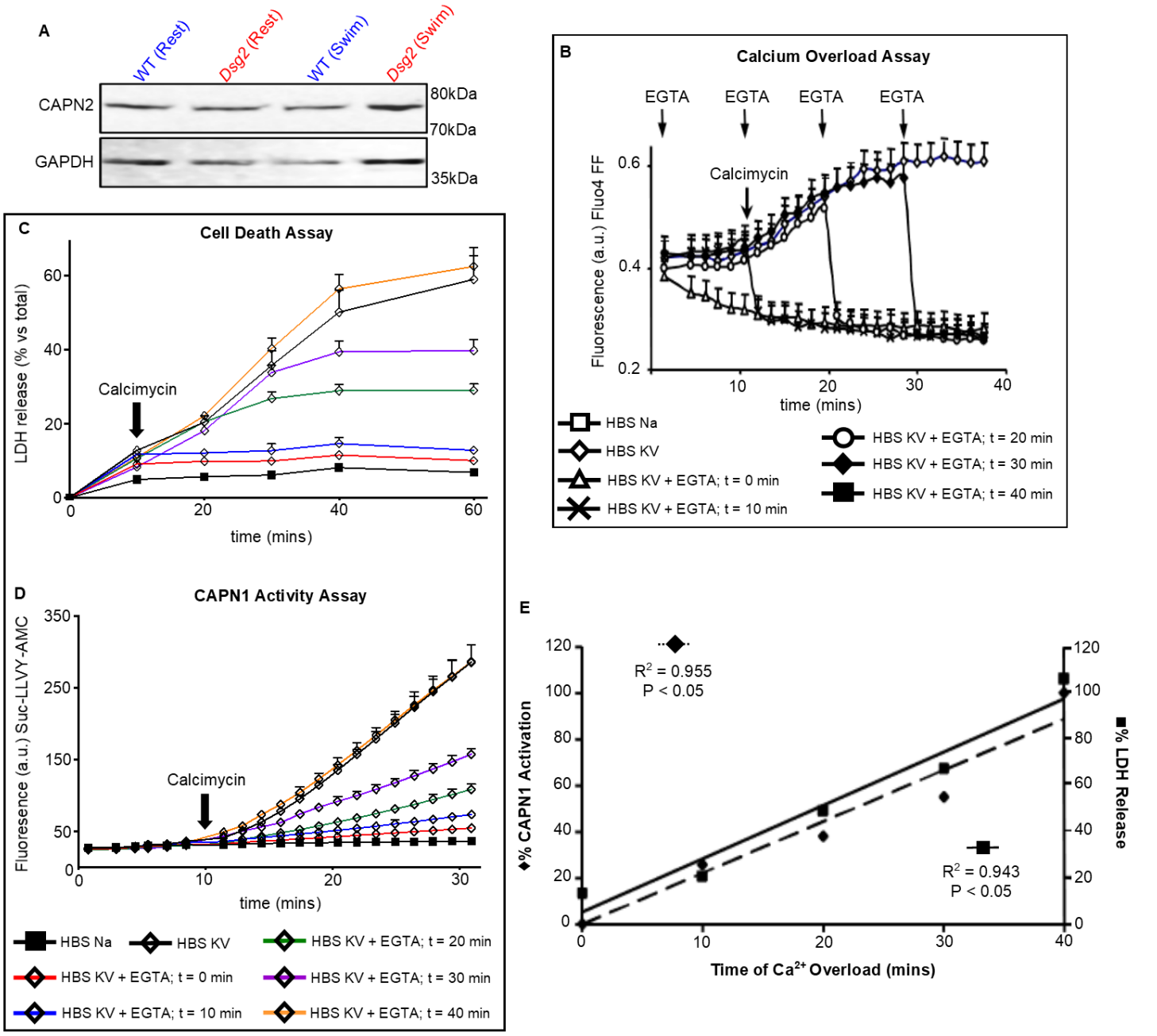

Fig. S2. CAPN1 activation and cell death in response to Ca^{2+} overload. (**A**) Representative Calpain-2 (CAPN2) immunoblot showed no difference in myocardial CAPN2 abundance from WT and *Dsg2*$^{mut/mut}$ (*Dsg2*) mice, in either sedentary or exercised cohorts. Data are representative of n = 7/genotype/cohort. (**B-E**) HL-1 cells were exposed to calcimycin (1 μM) to induce calcium (Ca^{2+}) overload and the Ca^{2+} chelating agent EGTA (5 mM) at the time points. Although not indicated explicitly on panels C and D, EGTA was added as shown in the key. (**B**) Cytosolic Ca^{2+} overload was detected by loading HL-1 cells with 5 μM Fluo4 FF. (**C**) Cell death was detected as lactate dehydrogenase (LDH) release. (**D**) CAPN1 activity was monitored through proteolytic cleavage of a synthetic CAPN1 peptide (Suc-LLVY-AMC) that produced a fluorescent signal. (**E**) Relationship between duration of Ca^{2+} overload (x-axis) with CAPN1 activation (%, solid diamonds; left y-axis) and with LDH release (%, solid squares; right y-axis). Both LDH release and CAPN1 activation are expressed as percentage of the maximal value obtained after 40 min of intracellular Ca^{2+} overload. Dotted line represents the relationship between duration of Ca^{2+} overload and CAPN1 activation. Solid line represents the relationship between duration of Ca^{2+} overload and LDH release. Pearson's r (R^2) correlation analyses and P-values are displayed within graph. In B-D, data are presented as mean ± SD (N = 6 independent experiments/cohort, with n = 3 cell culture replicates/condition).

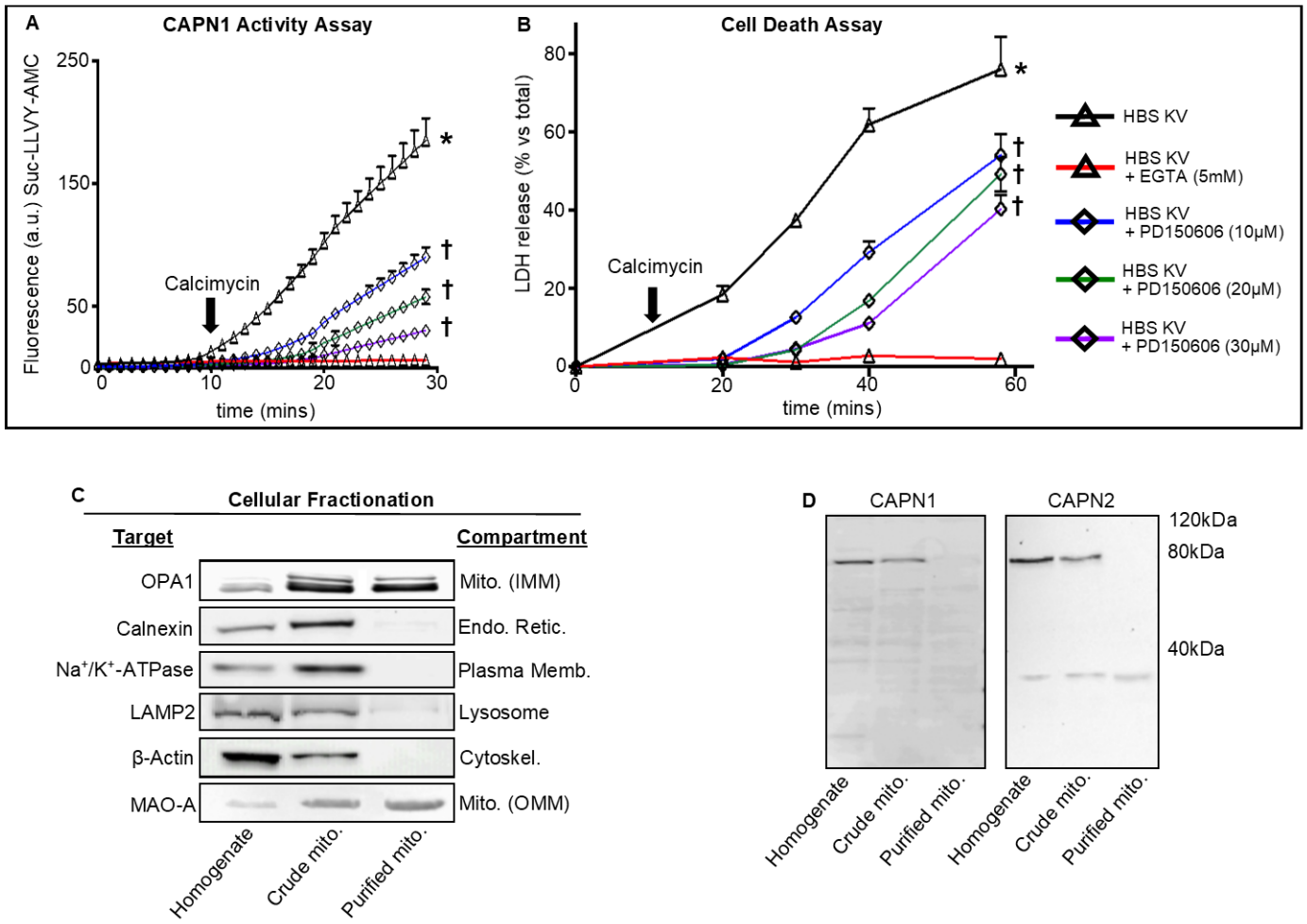

Fig. S3. CAPN1 inhibition in HL-1 cells by PD150606. HL-1 cells were subjected to Ca^{2+} overload with calcimycin in HBS KV medium in the absence or presence of the indicated concentrations of PD150606. (**A**) CAPN1 activity was monitored by proteolysis of the synthetic peptide Suc-LLVY-AMC (25 μM). (**B**) Cell death was detected as LDH release. Data presented as mean ± SD (N = 6 independent experiments/condition, with n = 3 cell culture replicates/condition; *, $P < 0.05$ for HBS KV media versus all conditions; †, $P < 0.05$ for HBS KV PD1050606 (10, 20, or 30 μM) media versus HBS KV media, using one-way ANOVA.) (**C**) Crude and purified fractions of mitochondria were obtained from HL-1 cells. Representative immunoblots of OPA1, calnexin, Na^+/K^+-ATPase, LAMP2, β-actin and MAO-A in protein extracts from total cell homogenate (lane 1), crude mitochondria (lane 2) and purified mitochondria (lane 3). Mito., mitochondria; IMM, inner mitochondrial membrane; Endo. Retic., endoplasmic reticulum; Plasma Memb., plasma membrane; Cytoskel., cytoskeleton; and OMM, outer mitochondrial membrane. (**D**) Representative immunoblots of antibodies recognizing domain IV of calpain-1 (CAPN1) or calpain-2 (CAPN2) in protein extracts from total cell homogenate (lane 1), crude mitochondria (lane 2), and purified mitochondria (lane 3) of HL-1 cells. For C, D, immunoblots are representative of N = 6 independent experiments/condition, with n = 3 cell culture replicates/condition.

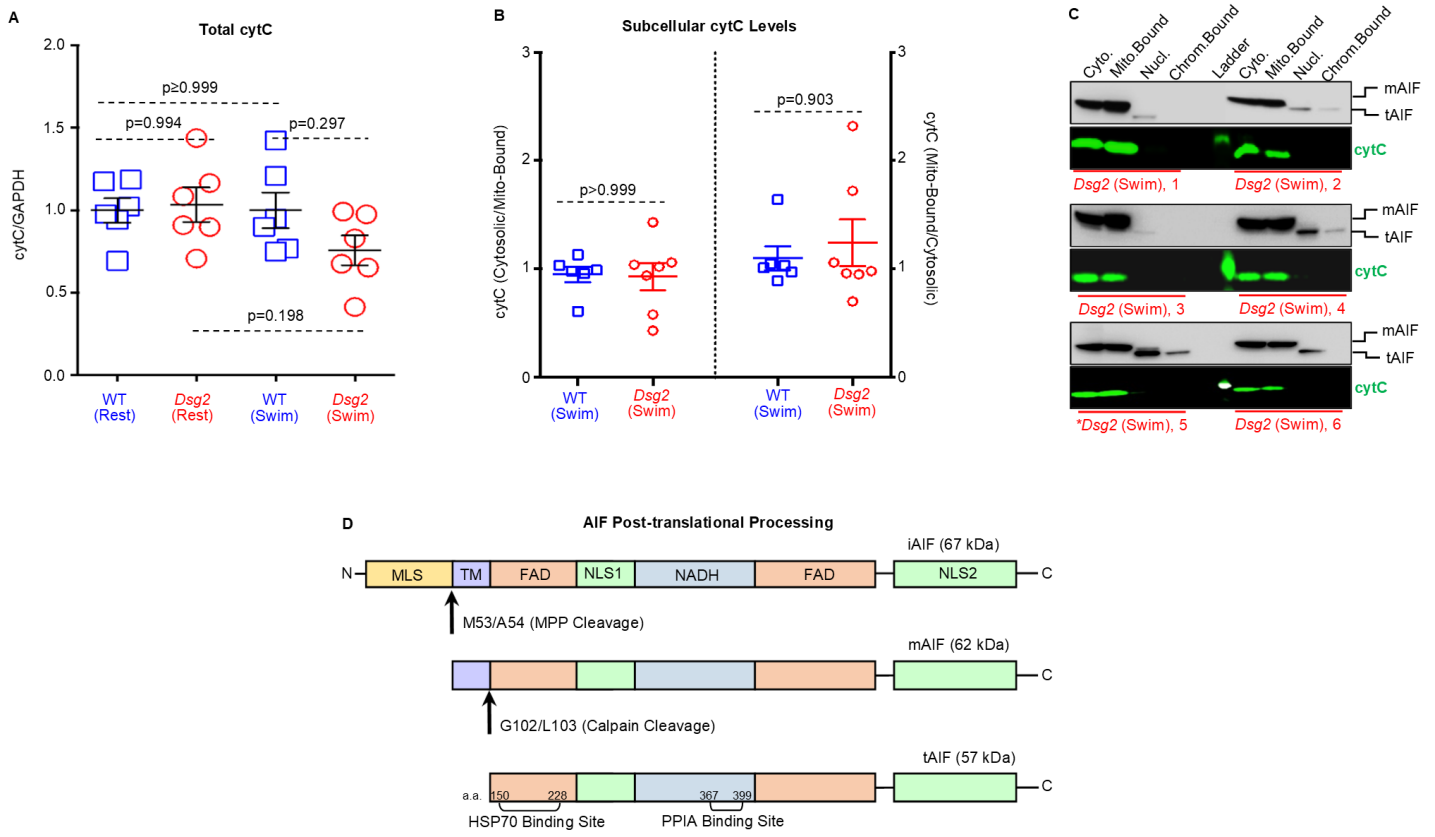

Fig. S4. CytC in *Dsg2*$^{mut/mut}$ mice and posttranslational modifications of AIF. (**A**) No differences in cytochrome-c (cytC) abundance were observed between cohorts, at rest or in response to exercise (swim). Data are presented as mean ± SEM (n = 6/cohort/condition with significance tested using one-way ANOVA). (**B**) Ratio of cytosolic-to-mitochondrial-bound cytC (left panel) or mitochondrial bound-to-cytosolic cytC in hearts from exercised cohorts. Data are presented as mean ± SEM (n ≥ 6 mice/cohort/condition with significance tested using one-way ANOVA with Tukey's post-hoc). (**C**) Representative myocardial immunoblots from individual exercised *Dsg2*$^{mut/mut}$ mice. **Dsg2* (Swim), 5 denotes the immunoblot that is also shown in Figure 4D. (**D**) Schematic showing immature AIF (iAIF) protein, posttranslational processing by MPP (mitochondrial processing peptidase), which promotes binding of mature AIF (mAIF) to the mitochondria inner membrane space. Calpain-cleavage generates truncated AIF (tAIF). MLS, mitochondrial localization signal; TM, transmembrane sequence that binds to mitochondrial intermembrane space; FAD/NADH domains; NLS, nuclear localization signal; M, A, G, and L are amino acids methionine, alanine, glycine, and leucine, respectively; a.a., amino acids; HSP70, heat shock protein-70; PPIA, cyclophilin-A.

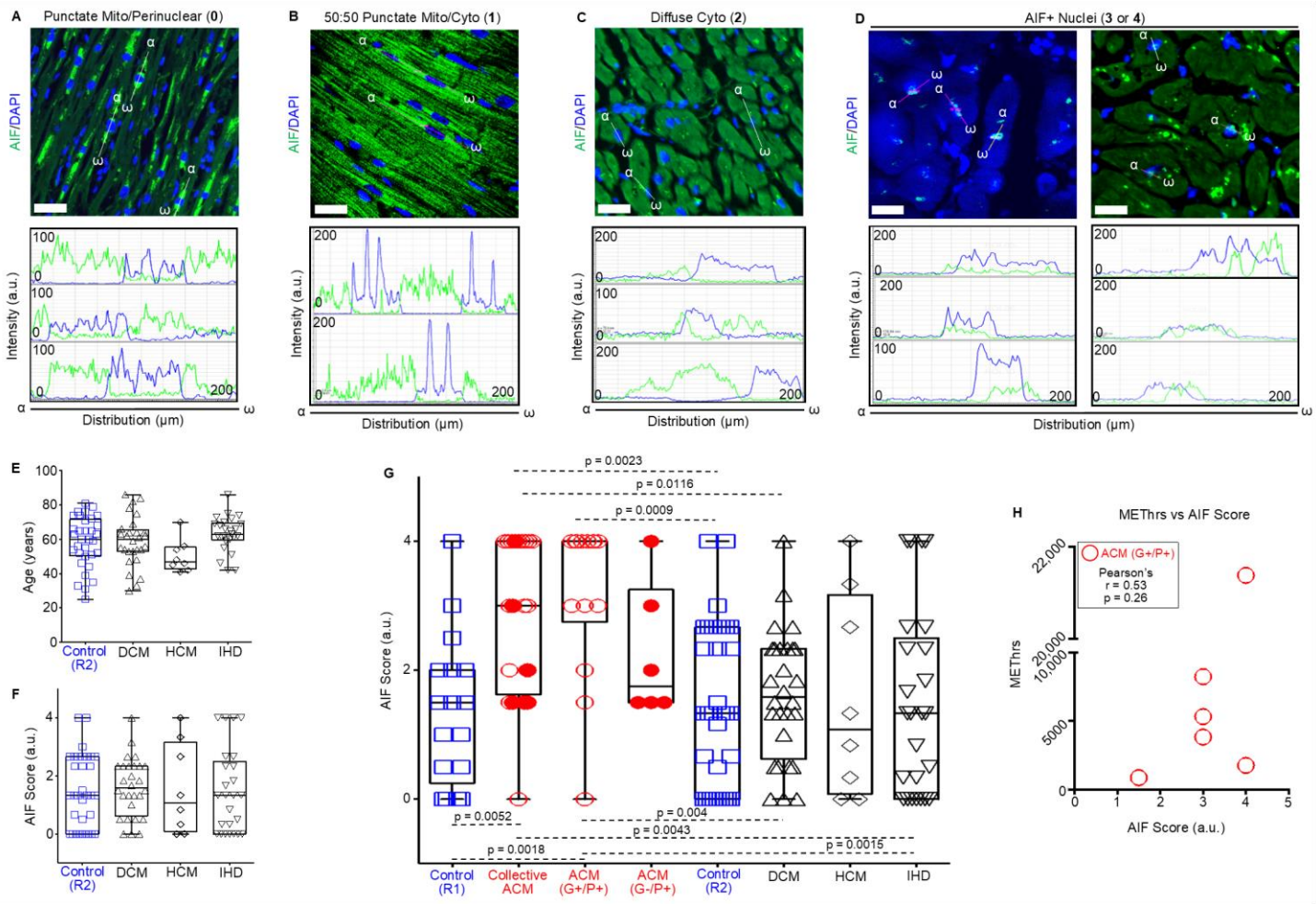

Fig. S5. AIF localization in ACM patient myocardium. Myocardium was given an AIF pathology score (Grade 0 – 4, number in bold within parentheses): (**A**) Grade 0 represents myocardia displaying robust punctate mitochondrial (mito) or perinuclear AIF, or both; (**B**) Grade 1 was assigned to myocardia with a 50:50 odds ratio of punctate mitochondrial AIF and diffuse cytosolic AIF (Mito/Cyto AIF); (**C**) Grade 2 was assigned to myocardia with diffuse cytosolic AIF and rare punctate AIF localization; (**D**) Grade 3 was assigned to myocardia with 2 – 3 nuclei positive for AIF (AIF+) and Grade 4 was assigned to myocardia with ≥ 4 AIF+ nuclei. Scale bars = 20 μm. (**E**) Age at biopsy, explant, or autopsy collection from tissue microarray (TMA). (**F**) AIF pathology scores. For E and F, data are presented as mean ± SEM, n = 33 controls (R2), n = 28 dilated cardiomyopathy (DCM), n = 8 hypertrophic cardiomyopathy (HCM), and n = 25 ischemic heart disease (IHD). No significant differences were found using one-way ANOVA with Tukey's posthoc. (**G**) AIF pathology scores in all cohorts. Data are presented as mean ± SEM, n = 17 controls (R1, controls from ACM analysis in Figure 7), n = 33 controls (R2, controls from the TMA analysis), n = 28 DCM, n = 8 HCM, n = 25 IHD, and n = 20 ACM (n = 14 ACM G+/P+; n = 6 ACM G-/P+). Significant differences were determined using one-way ANOVA with Tukey's posthoc. (**H**) Patient exercise history (METhrs) versus AIF pathology score using Pearson's correlation analysis.

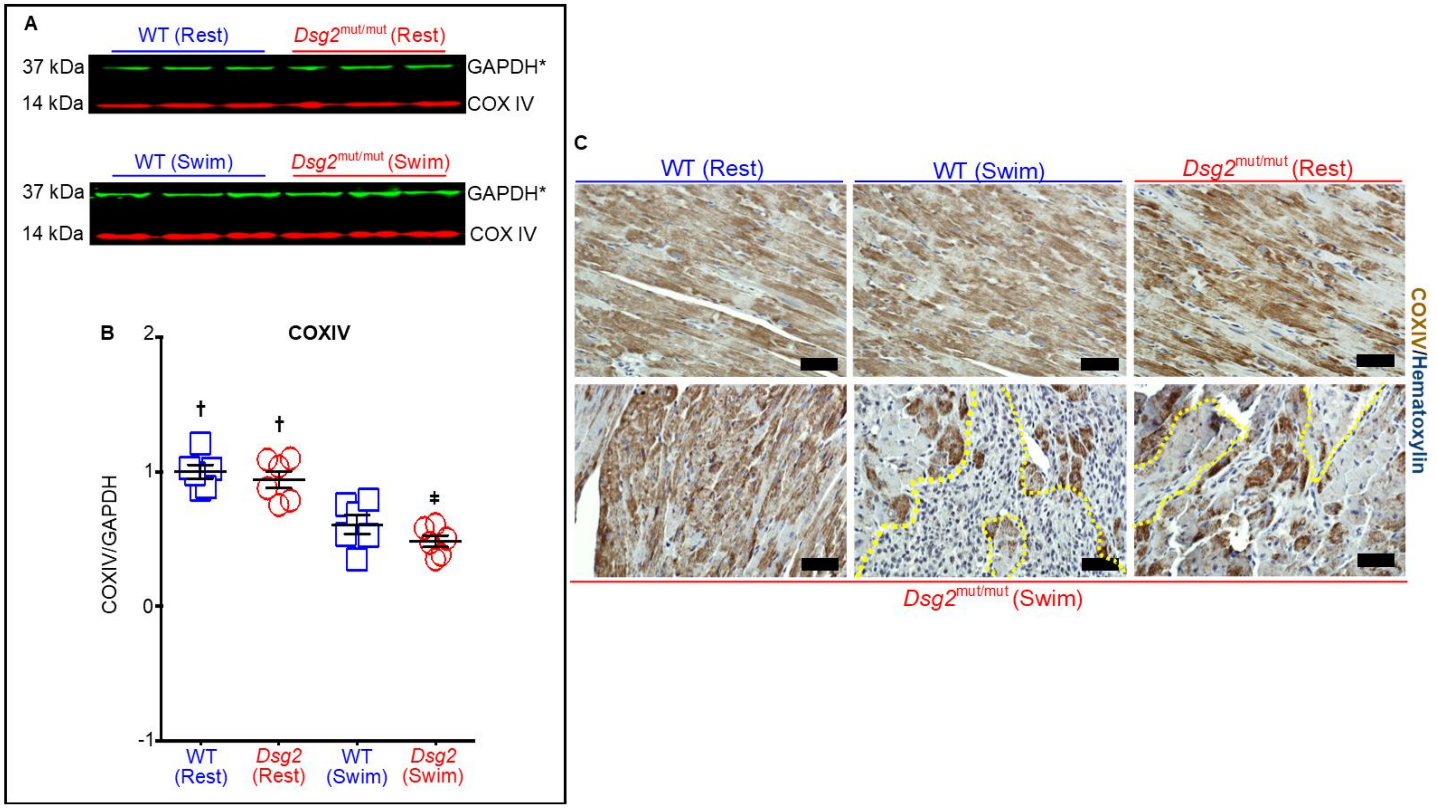

Fig. S6. *Dsg2*$^{mut/mut}$ mice display reduced COX IV abundance and aberrant myocardial localization. (**A, B**) Representative myocardial immunoblots and quantification of mitochondrial cytochrome-c oxidase (COX IV). *Denotes these immunoblots are also shown in Figure 3A. (Quantified data are presented as mean ± SEM [n = 6 mice/genotype/parameter; †, P < 0.05 any cohort versus WT (Swim); ‡, P < 0.05 *Dsg2*$^{mut/mut}$ (Swim) versus *Dsg2*$^{mut/mut}$ (Rest), using one-way ANOVA]. (**C**) Representative COX IV immunohistochemistry of myocardia from sedentary and exercised mice. Data are representative of n = 7/genotype/cohort. Scale bars = 100 µm.

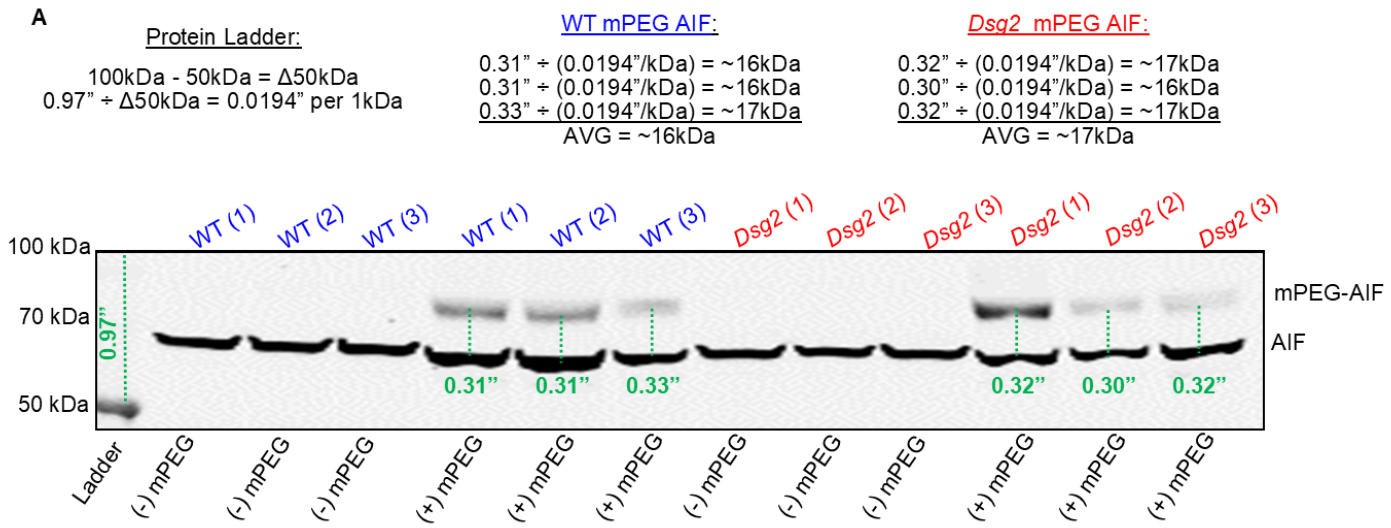

Fig. S7. Labeled cysteines and DNA gel electrophoresis. (**A**) Representative immunoblot of myocardial AIF from sedentary WT and *Dsg2*$^{mut/mut}$ mice with or without mPEG. The difference in the 100 – 50 kDa protein ladder (Δ50 kDa) divided by the length (in inches) between the 100-to-50kDa bands (0.97”) was used to determine the weight of mPEG-modified AIF. AIF contains 3 cysteines (regardless of its mature or truncated form). In the blot, after the molecular weight ladder, lanes 1 – 3 are untreated [(-) mPEG] myocardial lysates from 3 different WT mice [WT (1 – 3)] and lanes 4 – 6 are myocardial lysates incubated with 1 mM mPEG [(+) mPEG] from the same three WT mice from lanes 1 – 3. Lanes 7 – 9 are untreated [(-) mPEG] myocardial lysates from 3 different *Dsg2*$^{mut/mut}$ mice [*Dsg2* (1 – 3)] and lanes 10 – 12 are myocardial lysates incubated with 1 mM mPEG [(+) mPEG] from the same three *Dsg2*$^{mut/mut}$ mice from lanes 7 – 9. The length (in inches) indicated in green below represent the distances between non-modified AIF and mPEG labeled AIF.

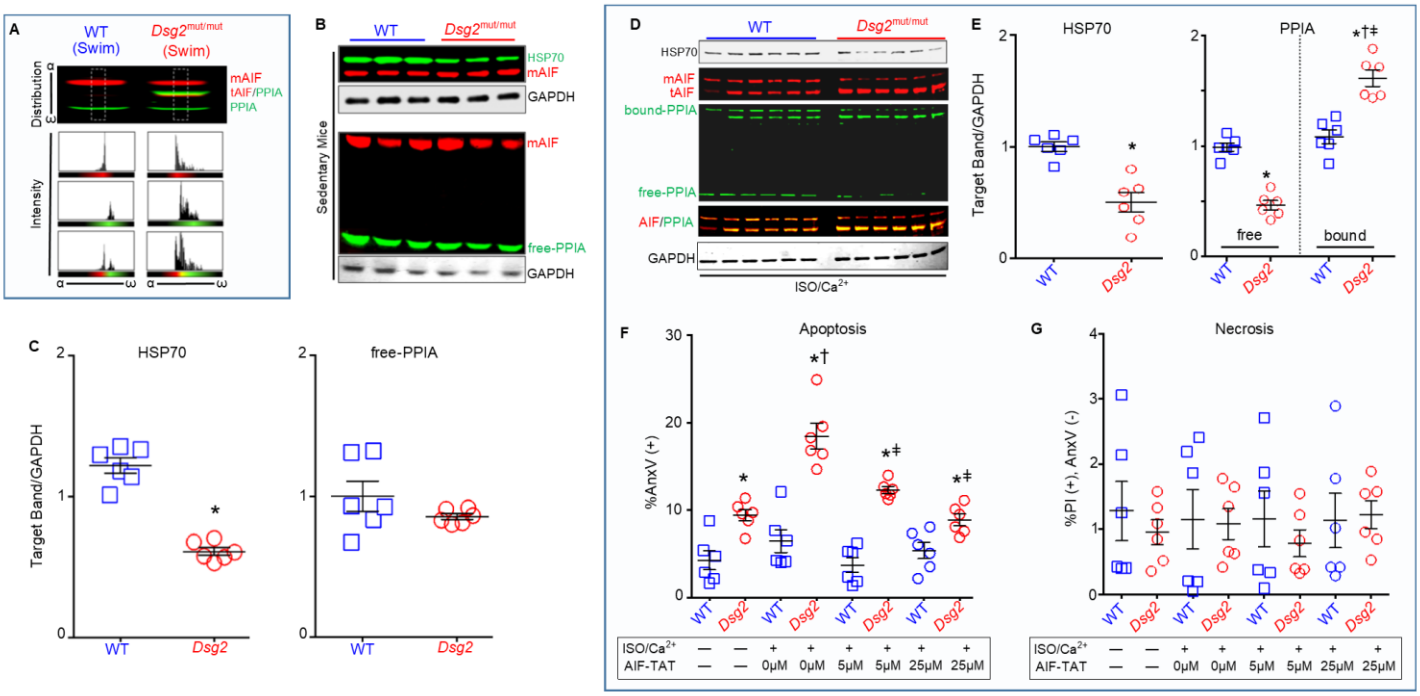

Fig. S8. HSP70 and PPIA abundance in ACM myocytes. (**A**) Representative immunoblot and corresponding histograms for the complex formed between AIF (red) and PPIA (green) using fluorophore distribution (α – ω). The overlap of both fluorophores (yellow) confirmed complex comigration. Immunoblot is from Figure 8A (lanes 3 and 4). (**B, C**) Immunoblots of the hearts from sedentary WT and *Dsg2*$^{mut/mut}$ mice probed for heat shock protein-70 (HSP70), AIF, and cyclophilin-A (PPIA). HSP70 and PPIA abundance was quantified. *, $P < 0.05$ *Dsg2*$^{mut/mut}$ (HSP70) versus WT (HSP70) using two-tailed paired t-test. (**D, E**) Representative immunoblots from ES-CMs treated for 7 days with 50 μM isoproterenol (ISO) and 1 μM calcium (Ca^{2+}) probed for PPIA, HSP70, and AIF. HSP70 and PPIA (free and bound to AIF) were quantified. *, $P < 0.05$ *Dsg2*$^{mut/mut}$ (HSP70) versus WT (HSP70) using two-tailed paired t-test. *, $P < 0.01$ *Dsg2*$^{mut/mut}$ (free or bound PPIA) versus WT (free PPIA); †, $P < 0.01$ *Dsg2*$^{mut/mut}$ (bound PPIA) versus WT (bound PPIA); ‡, $P < 0.01$ *Dsg2*$^{mut/mut}$ (bound PPIA) versus *Dsg2*$^{mut/mut}$ (free PPIA). (**F, G**) Flow cytometry analyses in ISO/Ca^{2+}-treated *Dsg2*$^{mut/mut}$ ES-CMs in the presence or absence of AIF-TAT mimetic peptide. *, $P < 0.05$ any group versus WT (no ISO/Ca^{2+}; no AIF-TAT); †, $P < 0.05$ any group versus *Dsg2*$^{mut/mut}$ (no ISO/Ca^{2+}; no AIF-TAT); ‡, $P < 0.05$ *Dsg2*$^{mut/mut}$ (5 μM or 25 μM AIF-TAT) versus *Dsg2*$^{mut/mut}$ (0 μM AIF-TAT), using one-way ANOVA with Tukey's post-hoc analysis. All quantified data are presented as mean ± SEM (n = 6/genotype/cohort/treatment).

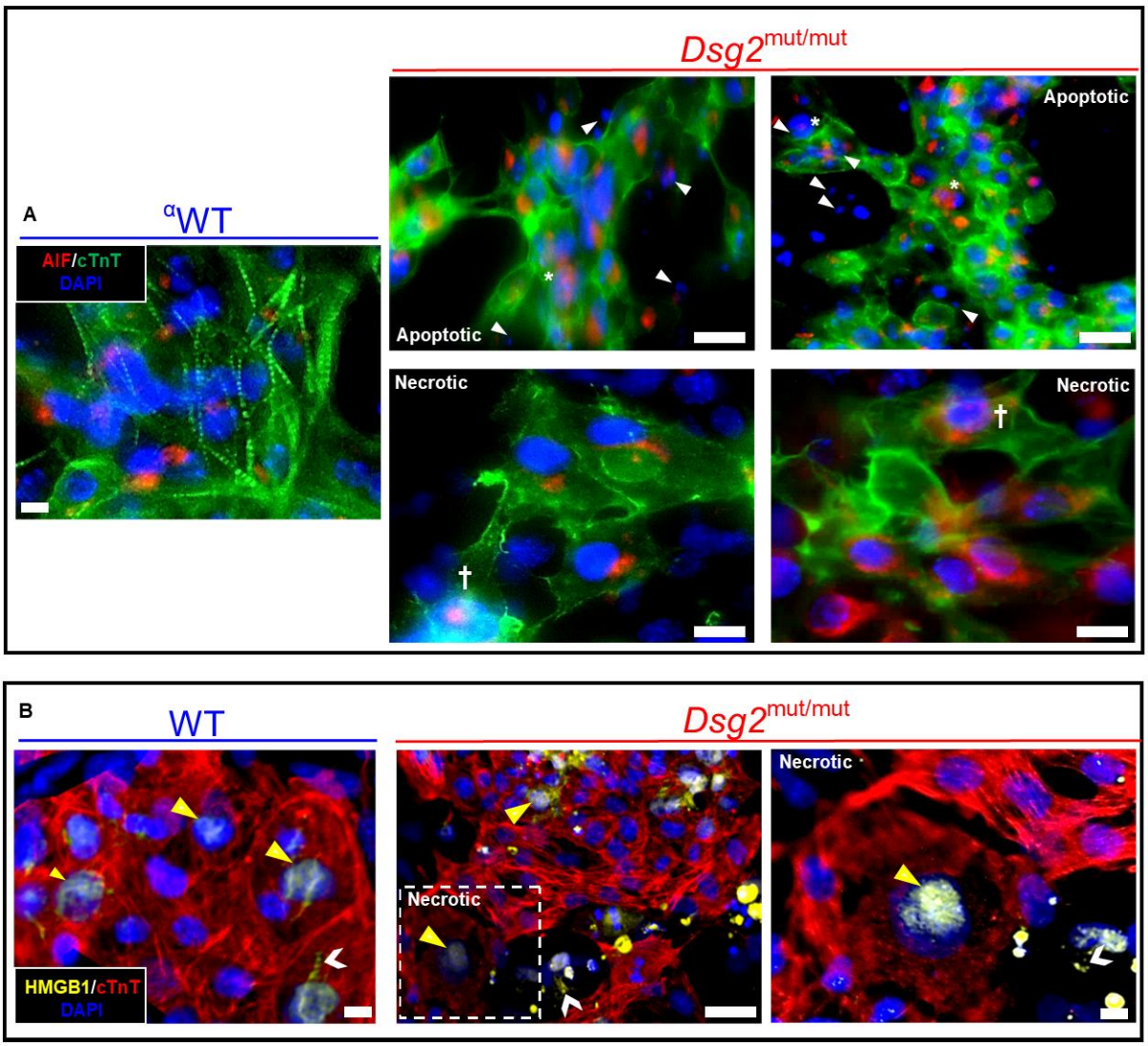

Figure S9. Increased AIF nuclear localization and nuclear loss of HMGB1 in ACM ES-CMs. (**A**) Representative images from WT and *Dsg2*$^{mut/mut}$ ES-CMs stimulated with ISO/Ca^{2+} for 7 days stained for AIF (red), cardiac troponin T (cTnT) (green), and DAPI (blue). White arrowheads, nuclear apoptotic bodies; white asterisk, AIF+ nuclei. $^{\alpha}$WT denotes the image is the same as that in Figure 8G. White cross, AIF+ nuclei. (**B**) Representative images from WT and *Dsg2*$^{mut/mut}$ ES-CMs stimulated with ISO/Ca^{2+} for 7 days stained for HMGB1 (yellow), cTnT (red), and DAPI (blue). Yellow arrowheads, HMGB1+ nuclei. White open arrowheads, nuclear loss of HMGB1. White dashed box is shown enlarged of a cell, with HMGB1+ nuclear staining, cell swelling, and enlargement of the nucleus, indicative of necrosis. Images are representative of N = 6 independent experiments/cohort, with n = 3 cell culture replicates/condition. Small scale bars = 25 μM; large scale bars = 50 μM

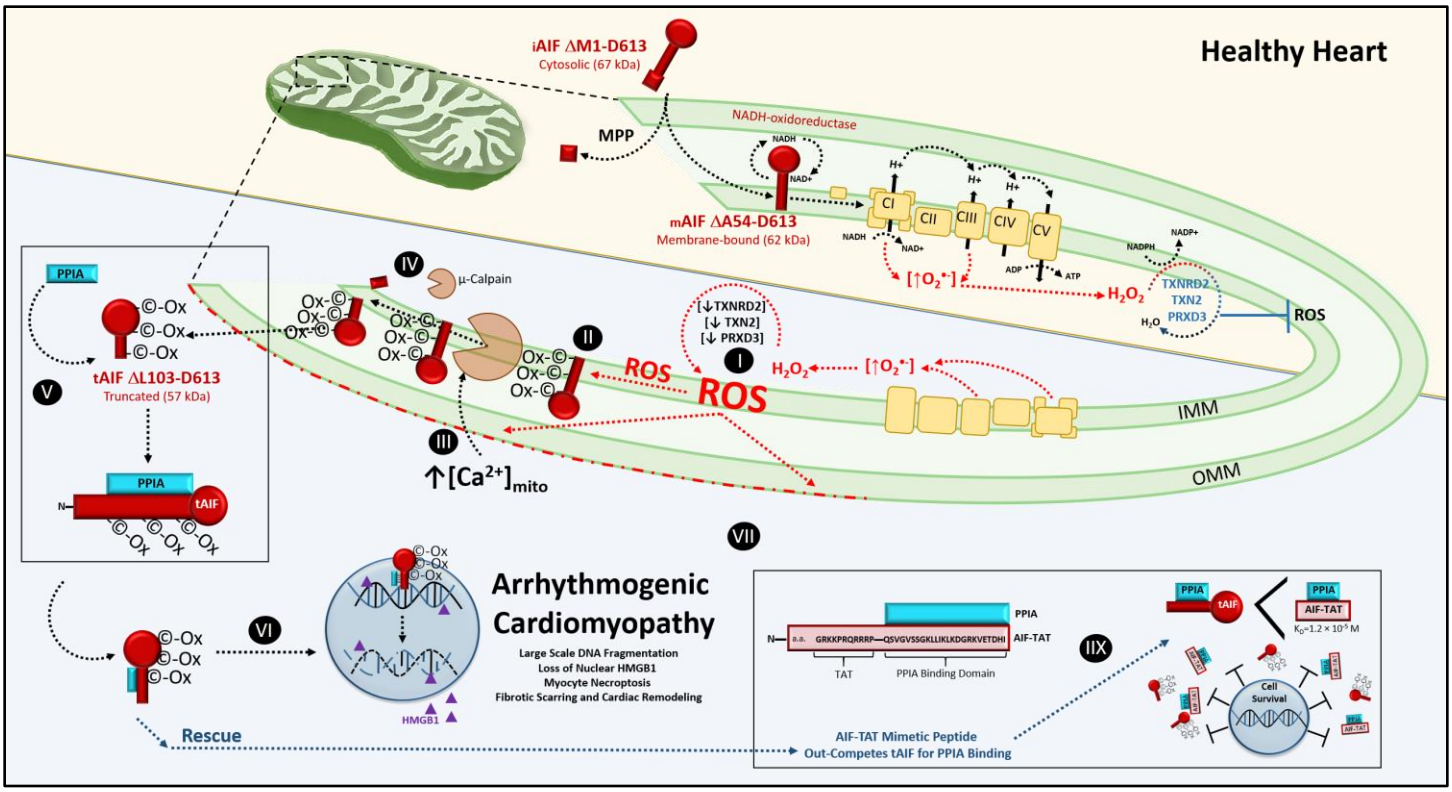

Fig. S10. Graphical abstract of exercise-induced, CAPN1/PPIA-mediated AIF-nuclear import in ACM. Top panel (yellow), Healthy Heart: cytosolic AIF (67kDa; amino acids: ΔMethionine [M1] – Aspartic Acid [D613]) is in its immature (iAIF) form when imported into the mitochondria. Where iAIF is cleaved by a mitochondrial processing peptidase (MPP) to form mature AIF (mAIF) where it is bound to the inner mitochondrial membrane (IMM). Mitochondrial-bound mAIF (62kDa; amino acids: ΔAlanine [A54]-D613) acts as an NADH-oxidoreductase recycling reducing equivalents (i.e., NADH/NAD+) back into the electron transport chain and additionally aids in Complex-I (CI) respiratory subunit assembly. Superoxide molecules ($O_2^{\bullet-}$) generated by CI and Complex-III (CIII) are converted to hydrogen peroxide (H_2O_2) via dismutation. Where in healthy mitochondria, hydrogen peroxide is reduced to water (H_2O) via the thioredoxin-2 (TXN2), TXN2-reductase (TXNRD2), peroxiredoxin-3 (PRXD3) system to prevent the formation of reactive oxygen species (ROS). Lower panel (blue), Arrhythmogenic Cardiomyopathy: (**I**) a depleted TXN2/TXNRD2/PRXD3 anti-ROS buffering system results in the accumulation of ROS, (**II**) where cysteine residues of mAIF are oxidized (-C-Ox) by augmented ROS levels. (**III**) Additionally, excessive ROS accumulation leads to permeabilization (red, intermittent dashed line) of the outer mitochondrial membrane (OMM), leading to outward solute leakage and inward calcium (Ca^{2+}) pumping. (**IV**) AIF undergoes a conformational change upon cysteine-oxidation, promoting Ca^{2+}-activated CAPN1 cleavage of Ox-mAIF to form truncated AIF (tAIF; 57kDa; amino acids: ΔLeucine [L103]-D613). (**V**) Oxidized, truncated AIF (Ox-tAIF) is liberated into the cytosol where cyclophilin-A (PPIA) binds to Ox-tAIF. (**VI**) PPIA-bound tAIF is transported to the myocyte nucleus where it causes large scale DNA fragmentation and nuclear loss of HMGB1. (**VII**) Utilizing an AIF-TAT mimetic peptide that mirrors the binding site of PPIA with a strong affinity to PPIA-binding (K_D = 1.2×10^{-5} M), (**IIX**) PPIA-mediated nuclear transport of tAIF can be prevented. Thereby, inhibiting AIF-induced necroptosis.

Table S1. Echocardiographic and electrocardiographic indices from exercised WT and *Dsg2*$^{mut/mut}$ mice.

Parameter	WT	*Dsg2*$^{mut/mut}$
Echocardiography		
n	20	15
IVSd (mm)	0.97 ± 0.02	0.78 ± 0.04*
IVSs (mm)	1.49 ± 0.04	1.08 ± 0.06*
LVIDd (mm)	2.80 ± 0.05	3.31 ± 0.19*
LVIDs (mm)	1.19 ± 0.06	2.24 ± 0.24*
RVIDd (mm)	1.16 ± 0.03	1.52 ± 0.07
RVIDs (mm)	0.42 ± 0.02	0.72 ± 0.06
LV-PWTd (mm)	0.94 ± 0.02	0.87 ± 0.03*
RV-PWTd (mm)	0.31 ± 0.01	0.32 ± 0.02
RVEF (%)	65.8 ± 0.73	54.9 ± 2.17*
LVEF (%)	81.6 ± 1.65	55.3 ± 4.61*
Electrocardiography		
n	13	13
PR-I (ms)	43.2 ± 2.2	45.7 ± 3.9
Pd (ms)	11.6 ± 0.7	10.8 ± 1.3
QRSd (ms)	16.7 ± 0.7	19.7 ± 1.1
P-Amp (mV)	0.10 ± 0.01	0.04 ± 0.01*
R-Amp (mV)	1.77 ± 0.14	1.49 ± 0.15
Q-Amp (mV)	-0.0003 ± 0.002	-0.12 ± 0.03*
S-Amp (mV)	-0.59 ± 0.05	-0.20 ± 0.03*
NSVT (count)	4.85 ± 1.4	21.9 ± 7.1*

Data are presented as mean ± SEM. Statistical differences between the mutant and WT hearts were determined by 1-way ANOVA (*, $P < 0.05$). IVS, interventricular septal end diastole (d) and end systole (s); LVID, left ventricular internal diameter; RVID, right ventricular internal diameter; LV-PWTd, LV posterior wall thickness; RV-PWTd, RV posterior wall thickness; PR-I, PR-Interval; Pd, P duration; QRSd, QRS duration; P-Amp, P-Amplitude; R-Amp, R-Amplitude; Q-Amp, Q-Amplitude; S-Amp, S-Amplitude. NSVT, non-sustained ventricular tachycardia.

Table S2. Desmosomal gene variants in patients with ACM. *PKP2* encodes plakophilin-2; *DSG2* encodes desmoglein-2.

Gene (n)	Nucleotide Change	Amino Acid Change	No. of Patients (n = 14)
PKP2 (12)	c.2509delA	p.Ser837Valfs*94	2
	c.148_151delACAG	p.Thr50Serfs*61	3
	c.2146-1G>C	mutant splice product	1
	c.2013delC	p.Pro672fs*12	2
	c.2489+1G>A	mutant splice product	2
	c.2197_2202delCACACCinsG	p.His733Alafs*8	1
	c.235C>T	p.Arg79*	1
DSG2 (2)	c.523+2T>C	mutant splice product	1
	c.918G>A c.146G>A	p.Trp306* p.Arg49His	1[a]

[a]Indicates patient with a compound heterozygote mutation in *DSG2*

Table S3. Clinical characteristics and AIF pathology scores of patients with ACM. Data are presented as mean ± SEM. P values were calculated with 2-way ANOVA.

AIF pathology score and clinical phenotypes	**Overall (n = 20)**	**G+/P+ (n = 14)**	**G-/P+ (n = 6)**	**P value**
AIF pathology score, mean ± SEM	2.90 ± 0.3	3.18 ± 0.3	2.25 ± 0.5	0.474
Proband, *n* (%)	13 (65)	9 (64)	4 (67)	> 0.999
Structural alterations, *n* (%)	12 (60) major 5 (25) minor	10 (71) major 2 (14) minor	2 (33) major 3 (50) minor	> 0.999
Repolarization abnormalities, *n* (%)	5 (25) major 9 (45) minor	4 (29) major 6 (43) minor	1 (17) major 3 (50) minor	> 0.999
Depolarization abnormalities, *n* (%)	17 (85) major 0 (0) minor	14 (100) major 0 (0) minor	3 (50) major 0 (0) minor	0.297
Arrhythmias, *n* (%)	7 (35) major 10 (50) minor	6 (43) major 7 (50) minor	1 (17) major 3 (50) minor	0.950

Data file S1. Raw data. (Excel file)